Prediction of the saturated hydraulic conductivity from Brooks and Corey's water retention parameters

Nasta, P.; Vrugt, J.A.; Romano, N.

DOI
10.1002/wrcr.20269

Publication date
2013

Document Version
Final published version

Published in
Water Resources Research

Prediction of the saturated hydraulic conductivity from Brooks and Corey's water retention parameters

Paolo Nasta,[1,2] Jasper A. Vrugt,[2] and Nunzio Romano[1]

Received 20 November 2012; revised 2 April 2013; accepted 18 April 2013; published 28 May 2013.

[1] Prediction of flow through variably saturated porous media requires accurate knowledge of the soil hydraulic properties, namely the water retention function (WRF) and the hydraulic conductivity function (HCF). Unfortunately, direct measurement of the HCF is time consuming and expensive. In this study, we derive a simple closed-form equation that predicts the saturated hydraulic conductivity, K_s from the WRF parameters of Brooks and Corey (1964). This physically based analytical expression uses an empirical tortuosity parameter (τ) and exploits the information embedded in the measured pore-size distribution. Our proposed model is compared against the current state of the art using more than 250 soil samples from the Grenoble soil catalog (GRIZZLY) and hydraulic properties of European soils (HYPRES) databases. Results demonstrate that the proposed model provides better predictions of the saturated hydraulic conductivity values with reduced size of the 90% confidence intervals of about 3 orders of magnitude.

Citation: Nasta, P., J. A. Vrugt, and N. Romano (2013), Prediction of the saturated hydraulic conductivity from Brooks and Corey's water retention parameters, *Water Resour. Res.*, *49*, 2918–2925, doi:10.1002/wrcr.20269.

1. Introduction

[2] Large-scale application of hydrological models requires explicit knowledge of the soil hydraulic properties, namely the soil water retention function (WRF) and the hydraulic conductivity function (HCF). The former is a relationship between the volumetric soil water content, θ (L^3 L^{-3}), and the soil matric pressure head, h (L), whereas the latter relates the soil hydraulic conductivity, K (L T^{-1}), to the soil water content or alternatively to the matric pressure head. Under full saturation, the values of θ and K are referred to as saturated water content (θ_s) and saturated hydraulic conductivity (K_s), respectively. Under very dry conditions, however, the amount of water that is immobilized in small aggregates or narrow pores and does not contribute to water flow is conventionally defined as the residual water content (θ_r). The physical interpretation of this parameter still remains rather ambiguous [*Haverkamp et al*., 2005; *Leij et al*., 2005].

[3] Even though conventional laboratory measurements of the WRF are generally practicable [*Dane and Hopmans*, 2002], direct determination of saturated hydraulic conductivity, K_s, and (unsaturated) HCF is rather time consuming, tedious, and expensive [*Hopmans et al*., 2002; *Schelle et al*., 2010; *Nasta et al*., 2011]. An alternative solution, which is especially useful for large-scale hydrological modeling, is to indirectly estimate the HCF using measurements of the pore-size distribution [*Peters and Durner*, 2006; *Dane et al*., 2011].

[4] As far as we are concerned, the work of *Childs and Collis-George* [1950] constitutes the first published contribution that predicts the unsaturated HCF from measurements of the soil water retention relationship, which in turn provides knowledge of the corresponding pore-size distribution. The soil is assumed to be made up of a bundle of capillary tubes of different radii and water flow is computed by combining Poiseuille's equation with Darcy's law [*Burdine*, 1953; *Brutsaert*, 1967]. The model proposed by *Mualem* [1976] represents the most refined approach of this kind and has been combined with popular analytical relationships to describe the WRF [*Brooks and Corey*, 1964; *van Genuchten*, 1980; *Kosugi*, 1996]. Bimodal water retention relationships have been introduced for structured soils to improve the prediction of the unsaturated hydraulic conductivity [*Durner*, 1994; *Tuller and Or*, 2002; *Dexter and Richard*, 2009; *Romano et al*., 2011].

[5] In this study we focus our attention to predict the saturated hydraulic conductivity, K_s, using parameters of the WRF. This study extends previous work on this topic [e.g., *Messing*, 1989; *Rawls et al*., 1998; *Timlin et al*., 1999; *Poulsen et al*., 1999; *Kawamoto et al*., 2006; *Han et al*., 2008]. Examples include the models proposed by *Mishra and Parker* [1990] and *Guarracino* [2007], and more recently *Matthews et al*. [2010]. All these models use the WRF of *van Genuchten* [1980]. Alternative approaches make use of Kozeny-Carman equation and derive the saturated hydraulic conductivity from some properties of the soil pores [*Carman*, 1939; *Ahuja et al*., 1984; *Ahuja et al*., 1989; *Chapuis and Aubertain*, 2003; *Green et al*., 2003; *Aminrun et al*., 2004].

[1]Department of Agriculture, Division of Agricultural, Forest and Biosystems Engineering, University of Napoli Federico II, Napoli, Italy.
[2]Department of Civil and Environmental Engineering, University of California, Irvine, California, USA.

Corresponding author: P. Nasta, Department of Agriculture, Division of Agricultural, Forest and Biosystems Engineering, University of Napoli Federico II, Napoli, I-80055, Italy. (paolo.nasta@unina.it)

0043-1397/13/10.1002/wrcr.20269

[6] The goal of the present study is to introduce a simple, yet robust closed-form equation that predicts the saturated hydraulic conductivity from Brooks and Corey's WRF parameters θ_s, h_b, and λ [*Brooks and Corey*, 1964]. For simplicity, the residual water content is assumed to be zero. The proposed model draws inspiration from the seminal work of *Childs and Collis-George* [1950] and infers the soil water flux from the pore-size distribution using $R_{\max}$ as the maximum effective pore radius (corresponding to the bubbling matric head, h_b, of Brooks-Corey's retention relation) [*Matthews et al*., 2010]. An empirical macroscopic tortuosity-connectivity calibration parameter, hereafter referred to as τ, is introduced to fit the measured K_s values.

[7] We compare the predictions of our model against those derived with the parametric relationships of *Mishra and Parker* [1990] and *Guarracino* [2007] using soil water retention and saturated hydraulic conductivity data from the Grenoble soil catalog (GRIZZLY) [*Haverkamp et al*., 1997; *Haverkamp et al*., 2005] and hydraulic properties of European soils (HYPRES) [*Wösten et al*., 1999; *Lilly et al*., 2008] databases.

2. Theory

2.1. Parametric Relations for Describing the Soil Water Retention Function

[8] We adopt a statistical approach and model the soil as a porous medium made up by a bundle of capillary tubes with radii, r (L) of different sizes that are randomly distributed with a probability function $p_{\mathrm{df}}(r)$ (L^{-1}). The term $p_{\mathrm{df}}(r)\mathrm{d}r$ (L^{-1} L) can be viewed as the fractional volume of pores with respect to the soil bulk volume. If these pores are completely filled with water, the volumetric water content, $\theta(r)$ is defined as

$$\theta(r) = \int_0^r p_{df}(r)\mathrm{d}r, \tag{1}$$

where the volume fraction of water is expressed as $\mathrm{d}\theta = p_{\mathrm{df}}(r)\mathrm{d}r$. By using the Young-Laplace equation, we can relate the pore radius, to the matric pressure head, h (L), and rewrite equation (1) as follows

$$\theta(h) = \int_{-\infty}^{h} p_{df}(r)\left(\frac{\mathrm{d}r}{\mathrm{d}h}\right)\mathrm{d}h = \int_{-\infty}^{h} f'(h)\mathrm{d}h, \tag{2}$$

where $f'(h) = \mathrm{d}\theta/\mathrm{d}h$ (L^{-1}) denotes the first derivative of the WRF, also known as the soil water capacity function. Once all pores are filled with water, the soil is saturated and the volumetric water content is defined as θ_s (L^3 L^{-3}). If the pore-size distribution is truncated up to the largest pore radius, hereafter referred to as $R_{\max}$ (L) and we assume that θ ($R_{\max}$) = θ_s, then

$$\theta_s = \int_0^{R_{\max}} p_{df}(r)\mathrm{d}r. \tag{3}$$

[9] To describe the soil WRF we use the parametric relation of *Brooks and Corey* [1964], hereafter referred to as BC-WRF

$$\theta(h) = (\theta_s - \theta_r)\left(\frac{h_b}{h}\right)^{\lambda} + \theta_r \text{ for } h < h_b, \tag{4a}$$

$$\theta(h) = \theta_s \text{ for } h_b \le h \le 0, \tag{4b}$$

where θ_r (L^3 L^{-3}) denotes the residual water content, h_b (L) is the bubbling matric head, and λ (-) characterizes the shape of the WRF. In practice, h_b is associated with the largest pore radius ($R_{\max}$) of the pore-size distribution since it defines the threshold at which the saturated soil starts draining and air replaces water into the void spaces. The parameter h_b is therefore also referred to as the air-entry value. For values of $h \ge h_b$, the soil pores are completely filled with water, and the soil hydraulic conductivity can be considered approximately constant and equal to K_s. If $h < h_b$ the hydraulic conductivity decreases nonlinearly with soil water content. Note that the residual water content is difficult to measure in practice, and is often estimated from extrapolation of the WRF to the (very) dry range [*Schelle et al*., 2010]. For mathematical convenience, we assume that $\theta_r = 0$. This leaves us with three parameters, θ_s, h_b, and λ that define the WRF.

2.2. Derivation of Predictive Model for K_s from Brooks and Corey's WRF

[10] If we mimic the soil as a bundle of N parallel nonintersecting capillary tubes with average (effective) radius r, then the total discharge Q (i.e., the volumetric water flow rate) (L^3 T^{-1}) flowing through this ideal porous medium can be computed from Poiseuille's law [*Hillel*, 1971]

$$Q = N\frac{\pi r^4 \rho_w g}{8\eta_w}J, \tag{5}$$

where J (L L^{-1}) denotes the hydraulic gradient between the edges of the tubes, g (L T^{-2}) represents the gravitational acceleration, and ρ_w (M L^{-3}) and η_w (M L^{-1} T^{-1}) signify the density and dynamic viscosity of the fluid (water), respectively.

[11] The specific discharge, q (L T^{-1}) through our hypothetical soil is defined as the total discharge per unit bulk cross-sectional area, A (L^2), and is mathematically equivalent to

$$q = \frac{Q}{A} = \frac{N\pi r^2}{A}\frac{r^2\rho_w g}{8\eta_w}J = \varepsilon_A\frac{r^2\rho_w g}{8\eta_w}J, \tag{6}$$

where $\varepsilon_A = N\pi r^2/A$ (L^2 L^{-2}) denotes the areal porosity. The assumption of a single effective pore radius for all N tubes is rather unrealistic. We therefore relax this assumption and assume that our hypothetical porous medium is made up of a bundle of nonintersecting straight cylindrical pores of length L_s, but with varying pore radii. If $\varepsilon_{A,i}$ represents the relative areal porosity of each pore-size class i, we can estimate the specific discharge as follows

$$q = \frac{\rho_w g}{8\eta_w} J \sum_{i=1}^{N_{ps}} \left(\varepsilon_{A,i} r_i^2\right), \tag{7}$$

where N_{ps} signifies the total number of pore-size classes between 0 and $R_{\max}$. If all pores are filled with water and contribute to flow, then this will lead to the specific discharge at full saturation.

[12] The fraction of water-filled pores, $\sum_{i=1}^{N_{ps}} \varepsilon_{A,i}$ can also be written in a more general continuous form by using equation (3). This leads to the following expression for the specific discharge

$$q = \frac{\rho_w g}{8\eta_w} J \int_0^{R_{\max}} p_{df}(r) r^2 \mathrm{d}r, \tag{8a}$$

which is equivalent to

$$q = \frac{\rho_w g}{8\eta_w} J \int_{-\infty}^{h_b} f'(h) \left(\frac{0.149}{h}\right)^2 \mathrm{d}h, \tag{8b}$$

with $r \approx 0.149/|h|$ at 20°C if expressing r in units of cm.

[13] A closer inspection of equation (8b) reveals that the specific discharge is quadratically proportional to the pore radius. Indeed, q will be influenced mostly by the largest pores that are predominantly generated by the aggregation and arrangement of the primary soil particles [*Durner*, 1994]. If we assume saturated conditions, then we can also use Darcy's Law to calculate the average water flux emanating from the soil sample

$$\overline{q} = K_s \overline{J}, \tag{9}$$

where $\overline{J}$ denotes the actual hydraulic gradient between the top and bottom of the porous medium. This macroscopic flux depends not only on the distribution of pore sizes (textural effect) and on the arrangement of the solid particles (structural effect), but also on the pore geometry and characteristics (tortuosity and connectivity effect) and on the physical properties of the fluid (viscosity and density effect) [*Corey*, 1994; *Dullien*, 1975; *Whalley et al.*, 2012]. The macroscopic water flux, $\overline{q}$ in equation (9) will therefore deviate from the specific discharge, q computed in equation (8b). To reconcile these differences, *Carman* [1956] proposed to pragmatically adjust the modeled specific discharge using

$$q = \overline{q}\left(\frac{L_a}{L_s}\right), \tag{10}$$

where L_a denotes the length of the tortuous path followed by the water particles under the actual hydraulic gradient, $\overline{J}$. If we now insert equation (10) into equation (8a), solve for $\overline{q}$ and subsequently combine this equation with equation (9), we yield the following expression for the saturated hydraulic conductivity, K_s

$$K_s \overline{J} = \frac{\rho_w g}{8\eta_w} J \left(\frac{L_s}{L_a}\right) \int_0^{R_{\max}} p_{df}(r) r^2 \mathrm{d}r, \tag{11}$$

[14] Friction losses are generally larger in and among the tortuous tubes. It is therefore reasonable to pose

$$\overline{J} = J\left(\frac{L_a}{L_s}\right), \tag{12}$$

which results in the following relation

$$K_s J \left(\frac{L_a}{L_s}\right) = \frac{\rho_w g}{8\eta_w} \left(\frac{L_s}{L_a}\right) \int_0^{R_{\max}} p_{df}(r) r^2 \mathrm{d}r, \tag{13}$$

in which we have assumed that $K_s \equiv K(R_{\max})$. This equation is equivalent to (see equations (8a) and (8b))

$$K_s = \frac{\rho_w g}{8\eta_w} \tau \int_{-\infty}^{h_b} f'(h) \left(\frac{0.149}{h}\right)^2 \mathrm{d}h, \tag{14}$$

where $\tau = (L_s/L_a)^2$ represents an empirical parameter $(0 < \tau < 1)$, commonly referred to as the macroscopic tortuosity-connectivity factor [*Carman*, 1956; *Bear*, 1972; *Vervoort and Cattle*, 2003].

[15] If we assume water at a temperature of 20°C, and thus $\rho_w = 0.998$ g cm^{-3}, h in units of cm, $\eta_w = 0.0102$ g cm^{-1} s^{-1}, and $g = 980.66$ cm s^{-2}, equation (14) can be written as follows

$$\begin{aligned} K_s = 4.315 \cdot 10^7 \tau \int_{-\infty}^{h_b} f'(h)(0.149/h)^2 \mathrm{d}h = 9.579 \\ \cdot 10^5 \tau \int_{-\infty}^{h_b} f'(h) \frac{1}{h^2} \mathrm{d}h, \end{aligned} \tag{15}$$

with K_s in cm h^{-1}.

[16] The first derivative, $f'(h)$ of the BC-WRF is computed analytically from equation (4a) for $h < h_b$

$$f'(h) = \frac{\mathrm{d}\theta}{\mathrm{d}h} = -\lambda \theta_s h_b^{\lambda} h^{(-\lambda-1)} = -\theta_s \frac{\lambda}{h_b} \left(\frac{h_b}{h}\right)^{(\lambda+1)}. \tag{16}$$

[17] By combining equations (15) and (16), the saturated hydraulic conductivity, K_s (cm h^{-1}) can now be calculated from the BC-WRF parameters

$$\begin{aligned} K_s &= -9.579 \cdot 10^5 \tau \lambda \theta_s h_b^{\lambda} \int_{-\infty}^{h_b} h^{-(\lambda+1)} \frac{1}{h^2} \mathrm{d}h \\ &= -9.579 \cdot 10^5 \tau \lambda \theta_s h_b^{\lambda} \int_{-\infty}^{h_b} h^{-(\lambda+3)} \mathrm{d}h \end{aligned}, \tag{17}$$

which after integration

$$\begin{aligned} K_s &= -9.579 \cdot 10^5 \tau \lambda \theta_s h_b^{\lambda} \left[-\frac{h^{-\lambda-2}}{\lambda+2}\right]_{-\infty}^{h_b} \\ &= 9.579 \cdot 10^5 \tau \frac{\lambda}{\lambda+2} \theta_s h_b^{\lambda} \left[\frac{1}{h^{\lambda+2}}\right]_{-\infty}^{h_b} \end{aligned}, \tag{18}$$

and rearranging leads to the following closed-form relation

$$K_s = 9.579 \cdot 10^5 \tau \frac{\lambda}{\lambda + 2} \frac{\theta_s}{h_b^2}, \quad (19)$$

with h_b in cm. This equation will be referred to as Model-Nasta, Vrugt, Romano (Model-NVR) in the remainder of this paper and the calculated K_s values will be denoted with $K_{s,\mathrm{NVR}}$.

2.3. Description of Two Other Existing Models to Predict K_s

[18] To demonstrate the advantages of the proposed model we compare the predictions of $K_{s,\mathrm{NVR}}$ derived with Model-NVR against those derived with the closed-form equations of *Guarracino* [2007] and *Mishra and Parker* [1990].

[19] These two alternative models both rely on the WRF proposed by *van Genuchten* [1980],

$$\theta(h) = \theta_r + (\theta_s - \theta_r)[1 + (\alpha|h|)^n]^{-m}, \quad (20)$$

where α (cm^{-1}), m (-), and n (-) are three shape parameters whose values need to be derived from calibration against the measured retention data. The value of m is typically derived through the common relationship, $m = 1 - 1/n$ [*Mualem*, 1976].

[20] *Guarracino* [2007] estimates the saturated hydraulic conductivity, $K_{s,\mathrm{G}}$ (cm h^{-1}) from the pore-size distribution using a fractal law distribution which is truncated between a minimum and a maximum pore radius. This simple model, hereafter referred to as Model-G, uses the following closed form equation

$$K_{s,\mathrm{G}} = 1.74 \cdot 10^5 \frac{2 - D}{4 - D} \theta_s \alpha^2, \quad (21)$$

with fractal dimension, D (-) originally set to 1.996, but considered a calibration parameter in the present analysis. This model uses only two parameters of the van Genuchten-water retention function (VG-WRF), α and θ_s and assumes the inverse of the air entry value, α^{-1} to identify the bubbling matric head, h_b.

[21] *Mishra and Parker* [1990] proposed the following parametric relationship, hereafter referred to as Model-MP, to estimate $K_{s,\mathrm{MP}}$ (cm h^{-1}) from the VG-WRF parameters α and θ_s

$$K_{s,\mathrm{MP}} = \frac{3.89 \cdot 10^5}{\tau_{\mathrm{MP}}} {\theta_s}^{5/2} \alpha^2, \quad (22)$$

with tortuosity factor, τ_{MP} (-) originally set at 2.5 [*Corey*, 1979] and considered constant.

[22] Table 1 summarizes the WRF and calibration parameters used in each of the three predictive models. In all our calculations, we assume that $\theta_r = 0$.

3. Soil Databases

[23] To evaluate the three predictive K_s models, we use 62 soil samples from the Grenoble soil catalog GRIZZLY [*Haverkamp et al.*, 1997; *Haverkamp et al.*, 2005] and 197 soil samples from the HYPRES database [*Wösten et al.*, 1999; *Lilly et al.*, 2008]. Data consist of soil bulk density, ρ_b (g cm^{-3}), texture classes (% clay, silt and sand), saturated water content, θ_s (cm^3 cm^{-3}), water retention data, $\theta(h)$ and saturated hydraulic conductivity $K_{s,\mathrm{obs}}$ (cm h^{-1}).

Table 1. Summary of the Three Different Models Used Herein With the WRF-Type (BC or VG), Number of Parameters (p), WRF Parameters and Empirical Parameters

	Model-NVR	Model-G	Model-MP
WRF	BC	VG	VG
p	3	2	2
WRF parameters	θ_s, λ, h_b	θ_s, α	θ_s, α
Empirical parameter	τ	D	τ_{MP}

[24] The U.S. department of agriculture texture distribution for the different soil samples is presented in Figure 1. All, but two texture classes (silty and sandy-clay) are represented. Quite conveniently, the GRIZZLY database includes estimates of the BC-WRF parameters, h_b (cm) and λ (-) and VG-WRF parameters, α (cm^{-1}), n (-), and m (-). For HYPRES the BC-WRF (equation (4)) and VG-WRF (equation (20)) parameters were derived by nonlinear optimization in MATLAB (the MathWorks, Inc.) [*Coleman and Li*, 1996]. Summary statistics of the soil properties and hydraulic parameters of both databases are reported in Table 2. The soil characteristics of both databases are quite similar, with the exception of K_s that differs considerably.

4. Results

4.1. Case Study I: The GRIZZLY Database

[25] Each of the three models considered herein contains a single empirical parameter, $\delta \in \{\tau, D, \tau_{\mathrm{MP}}\}$ that requires calibration against measured K_s data ($K_{s,\mathrm{obs}}$). We use the MATLAB Optimization Toolbox (The MathWorks, Inc.) [*Coleman and Li*, 1996], and calibrate each model by minimizing the sum of squared error (SSE) between ($\log_{10}$-transformed) observed, $K_{s,\mathrm{obs}}$ and predicted, $K_{s,\mathrm{pred}}$ saturated hydraulic conductivity values

$$\mathrm{SSE}(\delta) = \sum_{i=1}^{N_s} \left(\log_{10}\left[K^i_{s,\mathrm{obs}}\right] - \log_{10}\left[K^i_{s,\mathrm{pred}}(\delta)\right] \right)^2, \quad (23)$$

using the $N_s = 62$ samples of the GRIZZLY database.

[26] Table 3 lists the optimized values of the empirical parameters of Model-NVR, G, and MP, respectively, and their corresponding SSE values. Note that the optimal values of Model-G and Model-MP are comparable to their original (default) values of $D = 1.996$ and $\tau_{\mathrm{MP}} = 2.5$, respectively.

[27] We now evaluate the predictive capabilities of each individual model. The results are displayed in the left column of Figure 2 which shows a comparison between the observed and estimated K_s values for Model-NVR (Figures 2a and 2b), Model-G (Figures 2c and 2d) and Model-MP (Figures 2e and 2f). For convenience, the hydraulic conductivity values are plotted on a log-log scale (base-10) and the 1:1 line is graphically summarized (dashed line). The right column of Figure 2 plots histograms of the $\log_{10}$ transformed residuals.

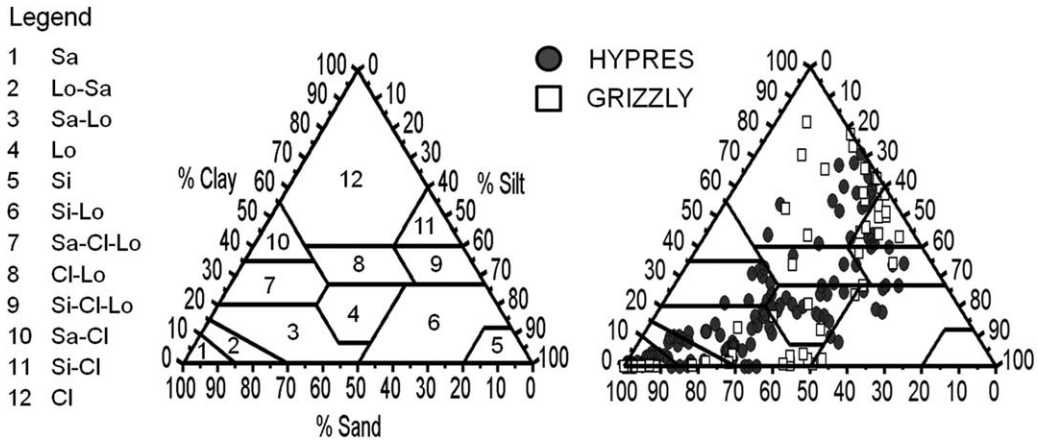

Figure 1. Soil texture distribution (Sa=sand; Lo=loam; Si=silt; Cl=clay) of the 62 soil samples of the GRIZZLY database (open squares) and of the 197 soil samples of the HYPRES database (solid circles).

[28] The left subplots in Figure 2 illustrate that the predictions of the proposed Model-NVR cluster most closely around the 1:1 line with 90% confidence intervals derived from a Student's t distribution (with $t = 1.671$ for $62-1=61$ degrees of freedom) that appear most tight. Model-MP exhibits the poorest performance, with the largest scatter and spread from all the three considered models. For all the three models the residuals are approximately Gaussian (according to the χ^2 test) and thus log-normally distributed. Model-G and Model-MP exhibit somewhat larger residuals than Model-NVR. Altogether, the results presented in Figure 2 thus favor the proposed Model-NVR for predicting the saturated hydraulic conductivity of the samples in the GRIZZLY database.

[29] The performance of the three models has also been quantified using simple summary statistics of the data fit. Table 3 lists the root mean square error (RMSE), the coefficient of determination (R^2), Akaike information criterion (AIC) and Bayes information criterion (BIC). All of the three models demonstrate a relatively good agreement between the predicted and observed K_s values with RMSE values that are smaller than 1 order of magnitude. Model-NVR exhibits the best performance with the lowest RMSE values, the highest R^2 and the smallest average spread of the 90% confidence limits. The AIC and BIC can be used to decide which of the three models is most favored given the available data. These two measures are defined through the following information criterion

$$I_i = -2\ln\left(L_{\max,i}\right) + \xi(p_i), \tag{24}$$

where $L_{\max}$ (L^2 T) is the (maximum) likelihood of model i and $\xi(p_i)$ represents a penalty term that penalizes for the number of parameters, p [*Diks and Vrugt*, 2010]. Indeed, the AIC and BIC diagnostics trade off quality of fit against model complexity. If the residuals are Gaussian distributed (see Figure 2), the value of $L_{\max}$ can be computed from the SSE using

$$-2\ln L_{\max} = N_s \ln\left(\frac{\mathrm{SSE}}{N_s - 1}\right) + N_s. \tag{25}$$

[30] The penalty term for AIC is $\xi(p) = 2p$ and for BIC this term is given by $\xi(p) = p\ln(N_s)$. The model with the lowest values for AIC and/or BIC is most supported by the available data. Note that AIC and BIC typically use the number of "calibration" parameters as measure of model complexity (penalty term). Each model used herein contains one empirical calibration parameter, and thus we can resort to metrics such as the RMSE and SSE to decide which model is statistically preferred. Yet we purposely

Table 2. Descriptive Statistics of the 62 Soil Samples of the GRIZZLY Database and 197 Samples of the HYPRES Database

		GRIZZLY				HYPRES			
Variables	Units	Mean	SD	Min	Max	Mean	SD	Min	Max
ρ_b	g cm^{-3}	1.35	0.33	0.97	1.91	1.58	0.16	0.95	1.86
Clay	%	25.4	27.5	0	81.6	18.7	20.5	0	71.0
Silt	%	28.6	17.2	0	55.1	23.3	17.3	0	60.4
Sand	%	45.9	36.5	0.3	100.0	58.0	33.6	0.8	100.0
θ_s	cm^3 cm^{-3}	0.43	0.077	0.27	0.61	0.39	0.063	0.27	0.61
$\log_{10}K_s$	cm h^{-1}	−0.72	1.21	−3.23	1.83	0.32	0.78	−1.71	2.25
$\log_{10} h_b$	cm	1.74	0.30	1.00	2.46	1.54	1.34	−0.97	2.00
λ		0.43	0.53	0.06	2.59	0.63	0.55	0.05	3.84
$\log_{10}\alpha$	cm^{-1}	−1.89	0.35	−2.65	−1.17	−1.64	0.34	−2.62	−0.34
n		1.62	0.91	1.08	5.54	1.72	0.55	1.08	4.71
m		0.27	0.21	0.072	0.82	0.37	0.16	0.075	0.79

Table 3. Calibrated Values of the Empirical Parameters (τ, D, and τ_{MP}) for Each of the Three Different Models (NVR, G, MP) Using the Samples From the GRIZZLY Data Set[a]

	Model-NVR	Model-G	Model-MP
Empirical parameter	$\tau = 0.0138$	$D = 1.9943$	$\tau_{MP} = 39.09$
SSE	35.54	47.41	60.67
RMSE	0.763	0.882	0.993
R^2	0.63	0.50	0.33
AIC	34.5	50.4	65.7
BIC	40.9	54.6	69.9

[a]Model fit is expressed by the sum of squared error (SSE), the root mean square error (RMSE), the coefficient of determination (R^2), Akaike's information criterion (AIC) and Bayes information criterion (BIC).

use the AIC and BIC to explicitly recognize differences in the number of input (WRF) parameters.

[31] Both the AIC and BIC listed in Table 3 indicate that Model-NVR is preferred over Model-G and Model-MP. In other words, the prediction of K_s is significantly improved by adding information about the pore-size distribution through the BC-WRF parameter λ.

4.2. Case Study II: The HYPRES Database

[32] To test the predictive performance of each of the three models we now use the HYPRES data set using the calibrated empirical parameters listed in Table 3. We graphically summarize the results in Figure 3 using a similar format as used previously in Figure 2. The left column compares measured and predicted hydraulic conductivities for each of the three considered parametric models, whereas the right column plots histograms of the associated error residuals.

[33] The scatter plots at the left hand side demonstrate that the observed K_s values of the HYPRES samples are substantially higher than those measured previously for the GRIZZLY samples (Table 2). This difference does not seem to affect the performance of the proposed Model-NVR. The RMSE of this model (0.78) is almost identical to its counterpart of 0.76 derived for the GRIZZLY database. This performance is significantly better than that of Model-G and Model-MP which exhibit RMSE values of 1.21 and 1.24, respectively.

[34] The predictions of Model-NVR group closely around the 1:1 line with 90% confidence intervals derived from Student's t distribution (with $t = 1.645$ for $197 - 1 = 196$

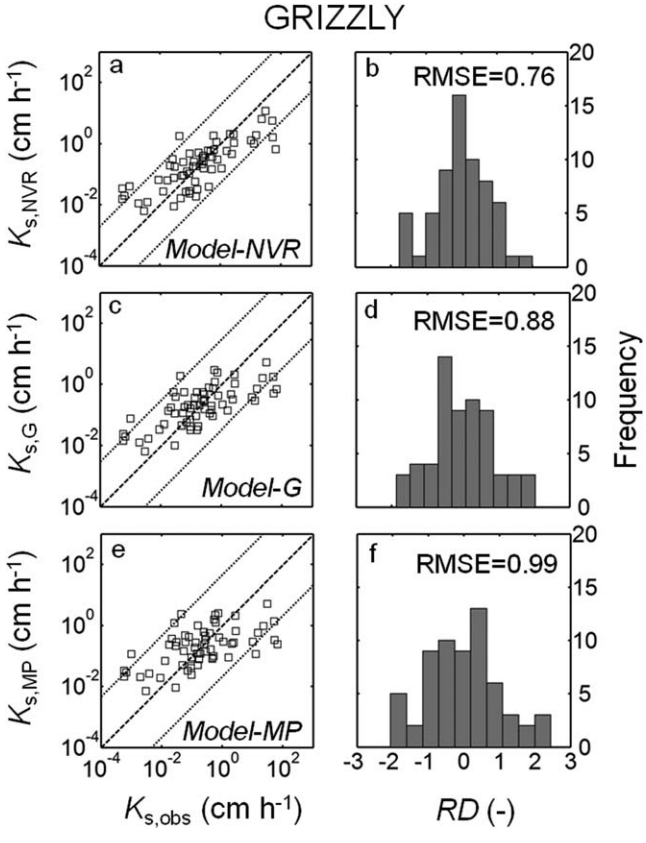

Figure 2. GRIZZLY database: Comparison between observed and predicted K_s values. Left column – Two-dimensional scatter plots of observed and predicted saturated hydraulic conductivities for models, (a) NVR, (c) G, and (e) MP. For convenience, we also include the 1:1 line (dashed line) and 90% confidence limits (dotted lines). Right column: Histograms of the corresponding residuals of the (b) NVR, (d) G, and (f) MP models.

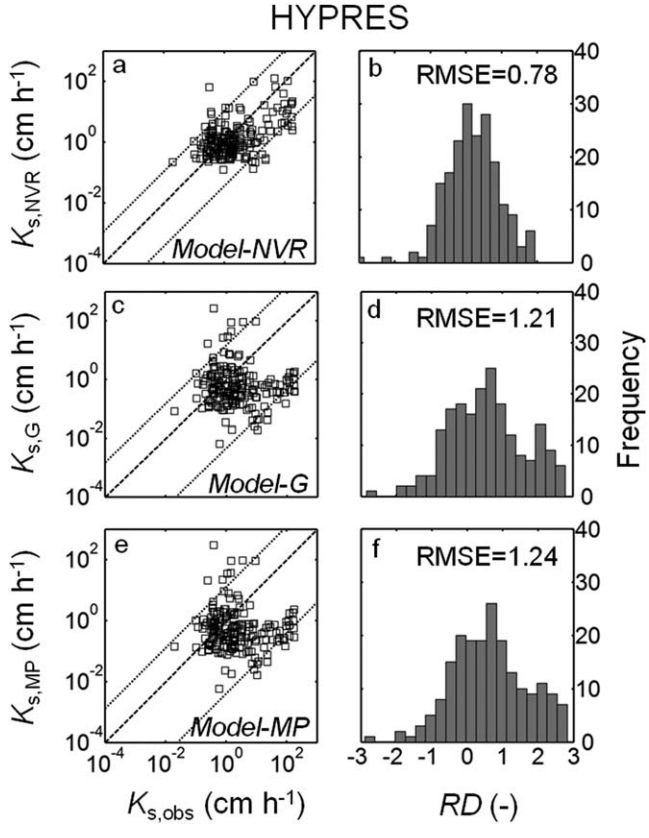

Figure 3. HYPRES database: Comparison between observed and predicted K_s values. Left column—Two-dimensional scatter plots of observed and predicted saturated hydraulic conductivities for models, (a) NVR, (c) G, and (e) MP. The 1:1 line (dashed line) and 90% confidence limits (dotted lines) are conveniently included. Right column: Histograms of the corresponding residuals of the (b) NVR, (d) G, and (f) MP models.

Table 4. Performance of Each of the Three Prediction Models (NVR, G, MP) Using the 197 Soil Samples From the HYPRES Data Set[a]

	Model-NVR	Model-G	Model-MP
SSE	118.17	285.61	300.96
RMSE	0.776	1.207	1.239
R^2	0.31	0.17	0.12
AIC	103.3	275.2	285.5
BIC	109.7	279.4	289.7

[a]The empirical parameters (τ, D, and τ_{MP}) have been set to their calibrated values in Table 3. The model fit is expressed with the sum of squared error (SSE), the root mean square error (RMSE), the coefficient of determination (R^2), Akaike's information criterion (AIC) and Bayes information criterion (BIC).

degrees of freedom) which are substantially smaller than those derived with the other two models. Moreover, the histograms of the (log)-residuals computed with Model-NVR center around zero, whereas a significant bias is observed for the other two models. Altogether these results demonstrate an improved ability of Model NVR to predict the measured K_s values.

[35] This conclusion is further supported by the summary diagnostics of the model fits listed in Table 4. Note, however that all of the three models exhibit a relatively low coefficient of determination (R^2). This highlights that "single-average" calibrated values of the empirical parameters cannot fully capture the observed variation. The AIC and BIC criteria once again indicate that the exploitation of all WRF parameters (θ_s, h_b, and λ) in the proposed Model-NVR has desirable statistical advantages. The fit to the observed K_s data is significantly enhanced and the prediction uncertainty reduced.

4. Conclusion

[36] When direct measurement of the saturated hydraulic conductivity is not affordable, it is necessary to use an alternative approach that predicts the K_s values from available soil hydraulic properties. In this paper we introduced a simple but robust closed-form parametric relation that predicts the saturated hydraulic conductivity from the BC water retention parameters. The proposed model not only significantly improves the prediction of the saturated hydraulic conductivity, but the associated confidence intervals are also considerably smaller. We posit that further improvements are possible, if the procedure for the calibration of τ is further refined.

Notation

A Bulk cross-sectional area of the soil, L^2
D Fractal dimension in Model-G
$f'(h)$ Water capacity function, L^{-1}
g Gravitational acceleration, $L\ T^{-2}$
h Matric suction head, L
h_b Bubbling matric head of the BC-WRF, L
I Information criterion
J Hydraulic gradient, $L\ L^{-1}$
K Hydraulic conductivity, $L\ T^{-1}$
K_s Saturated hydraulic conductivity, $L\ T^{-1}$
L_s Straight length of the bundle of cylindrical pores, L
L_a Actual length of the bundle of cylindrical pores, L
L_{max} Maximum likelihood, $L^2\ T$
m Shape parameter of the VG-WRF
N Number of capillary pores
N_s Number of samples
N_{ps} Number of pore-size classes
n Shape parameter of the VG-WRF
p Number of parameters
$p_{df}(r)$ Probability distribution function of pores, L^{-1}
Q Volumetric flow rate, $L^3\ T^{-1}$
q Specific discharge, $L\ T^{-1}$
r Pore radius, L
R_{max} Maximum pore radius, L
α Shape parameter of the VG-WRF, L^{-1}
ε_A Soil areal porosity, $L^2\ L^{-2}$
η_w Dynamic viscosity of water, $M\ L^{-1}\ T^{-1}$
λ Pore-size distribution index of the BC-WRF
ρ_w Water density, $M\ L^{-3}$
τ Macroscopic tortuosity-connectivity in Model-NVR
τ_{MP} Tortuosity in the Model-MP
ξ Penalty term in the information criterion
θ Soil water content, $L^3\ L^{-3}$
θ_r Residual water content, $L^3\ L^{-3}$
θ_s Saturated water content, $L^3\ L^{-3}$

[37] **Acknowledgments.** The authors wish to thank R. Haverkamp and A. Lilly for graciously providing the GRIZZLY and HYPRES data sets. We also acknowledge the comments and suggestions of W. Durner and two anonymous reviewers that have enhanced the quality of the current version of this paper.

References

Ahuja, L. R., J. W. Naney, P. E. Green, and D. R. Nielsen (1984), Macroporosity to characterize spatial variability of hydraulic conductivity and effects of land management, *Soil Sci. Soc. Am. J.*, *48*, 699–702.

Ahuja, L. R., D. K. Cassel, R. R. Bruce, and B. B. Barns (1989), Evaluation of spatial distribution of hydraulic conductivity using effective porosity data, *Soil Sci.*, *148*, 404–411.

Aminrun, W., M. M. Amin, and S. M. Eltaib (2004), Effective porosity of paddy soils as an estimate of its saturated hydraulic conductivity, *Geoderma*, *121*, 197–203.

Bear, J. (1972), *Dynamics of Fluids in Porous Media*, Elsevier, New York.

Brooks, R. H., and A. T. Corey (1964), Hydraulic properties of porous media, in *Hydrology Paper No. 3*, 27 pp., Colorado State Univ., Fort Collins, Colo.

Brutsaert, W. (1967), Some methods of calculating unsaturated permeability, *Trans. ASAE*, *10*, 400–404.

Burdine, N. T. (1953), Relative permeability calculation size distribution data, *Trans. Am. Inst. Min. Metall. Pet. Eng.*, *198*, 71–78.

Carman, P. C. (1939), Permeability of sands soils and clays, *J. Agric. Sci.*, *29*, 262–273.

Carman, P. C. (1956), *Flow of Gases through Porous Media*, Academic, New York.

Chapuis, R. P., and M. Aubertin (2003), On the use of Kozeny-Carman equation to predict the hydraulic conductivity of soils, *Can. Geotech. J.*, *40*, 616–628.

Childs, E. C., and N. Collis-George (1950), The permeability of porous materials, *Proc. R. Soc. A*, *201*, 392–405.

Coleman, T. F., and Y. Li (1996), An interior, trust region approach for nonlinear minimization subject to bounds, *SIAM J. Optim.*, *6*, 418–445.

Corey, A. T. (1979), *Mechanics of Heterogeneous Fluids in Porous Media (Reprinted 2003)*, Water Resour. Publ., Littleton, Colo.

Corey, A. T. (1994), *Mechanics of Immiscible Fluids in Porous Media (Reprinted 2003)*, Water Resour. Publ., Highlands Ranch, Colo.

Dane, J. H., and J. W. Hopmans (2002), Water retention and storage, in *Methods of Soil Analysis, Part 4, SSSA Book Ser. 5*, edited by J. H. Dane and G. C. Topp, pp. 671–675, SSSA, Madison, Wis.

Dane, J. H., J. A. Vrugt, and E. Unsal (2011), Soil hydraulic functions determined from measurements of air permeability, capillary modeling and high-dimensional parameter estimation, *Vadose Zone J.*, *10*, 1–7.

Dexter, A. R., and G. Richard (2009), The saturated hydraulic conductivity of soils with n-modal pore-size distributions, *Geoderma*, *154*, 76–85.

Diks, C. G. H., and J. A. Vrugt (2010), Comparison of point forecast accuracy of model averaging methods in hydrologic applications, *Stochastic Environ. Res. Risk Assess.*, *24*, 809–821.

Dullien, F. A. L. (1975), Single phase flow through porous media and pore structure, *Chem. Eng. J.*, *10*, l–34.

Durner, W. (1994), Hydraulic conductivity estimation for soils with heterogeneous pore structure, *Water Resour. Res.*, *30*, 211–223.

Green, T. R., L. R. Ahuja, J. G. Benjamin (2003), Advances in predicting agricultural management effects on soil hydraulic properties, *Geoderma*, *116*, 3–27.

Guarracino, L. (2007), Estimation of saturated hydraulic conductivity Ks from the van Genuchten shape parameter α, *Water Resour. Res.*, *43*, W11502, doi:10.1029/2006WR005766.

Han, H., D. Giménez, and A. Lilly (2008), Textural averages of saturated soil hydraulic conductivity predicted from water retention data, *Geoderma*, *146*, 121–128.

Haverkamp, R., C. Zammit, F. Boubkraoui, K. Rajkai, J. L. Arrúe, and N. Heckmann (1997), *GRIZZLY, Grenoble soil catalogue: Soil survey of field data and description of particle-size, soil water retention and hydraulic conductivity functions*, Lab. d'Etude des Transferts en Hydrol. et en Environ., Grenoble, France.

Haverkamp, R., F. J. Leij, C. Fuentes, A. Sciortino, and P. J. Ross (2005), Soil water retention: I. Introduction of a shape index, *Soil Sci. Soc. Am. J.*, *69*, 1881–1890.

Hillel, D. (1971), *Soil and Water: Physical Principles and Processes*, Academic, New York.

Hopmans, J. W., J. Šimůnek, N. Romano, and W. Durner (2002), *Inverse methods, in Methods of Soil Analysis, Part 4, SSSA Book Ser. 5*, edited by J. H. Dane and G. C. Topp, pp. 963–1008, SSSA, Madison, Wis.

Kawamoto, K., P. Moldrup, T. P. A. Ferre, M. Tuller, O. H. Jacobsen, and T. Komatsu (2006), Linking the Gardner and Campbell models for water retention and hydraulic conductivity in near—Saturated soil, *Soil Sci.*, *171*, 573–584, doi:10.1097/01.ss.0000228035.72647.3c.

Kosugi, K. (1996), Log-normal distribution model for unsaturated soil hydraulic properties, *Water Resour. Res.*, *32*, 2697–2703.

Leij, F. J., R. Haverkamp, C. Fuentes, Z. Zatarain, and P. J. Ross (2005), Soil water retention: II. Derivation and application of shape index, *Soil Sci. Soc. Am. J.*, *69*, 1891–1901.

Lilly, A., A. Nemes, W. J. Rawls, and Y. A. Pachepsky (2008), Probabilistic approach to the identification of input variables to estimate hydraulic conductivity, *Soil Sci. Soc. Am. J.*, *72*, 16–24.

Matthews, G. P., G. M. Laudone, A. S. Gregory, N. R. A. Bird, A. G. D. G. Matthews, and W. R. Whalley (2010), Measurement and simulation of the effect of compaction on the pore structure and saturated hydraulic conductivity of grassland and arable soil, *Water Resour. Res.*, *46*, W05501, doi:10.1029/2009WR007720.

Messing, I. (1989), Estimation of saturated hydraulic conductivity in clay soils from moisture retention data, *Soil Sci. Soc. Am. J.*, *53*, 665–668.

Mishra, S., and J. C. Parker (1990), On the relation between saturated conductivity and capillary retention characteristics, *Ground Water*, *28*, 775–777.

Mualem, Y. (1976), A new model for predicting the hydraulic conductivity of unsaturated porous media, *Water Resour. Res.*, *12*, 513–522.

Nasta, P., S. Huynh, and J. W. Hopmans (2011), Simplified multistep outflow method to estimate unsaturated hydraulic functions for coarse-textured soils, *Soil Sci. Soc. Am. J.*, *75*, 418–425.

Peters, A., and W. Durner (2006), Improved estimation of soil water retention characteristics from hydrostatic column experiments, *Water Resour. Res.*, *42*, W11401, doi:10.1029/2006WR004952.

Poulsen, T. G., P. Moldrup, T. Yamaguchi, and O. H. Jacobsen (1999), Predicting saturated and unsaturated hydraulic conductivity in undisturbed soils from soil water characteristics, *Soil Sci.*, *164*, 877–887.

Rawls, W. J., D. Gimenez, and R. Grossman (1998), Use of soil texture, bulk density, and slope of the water retention curve to predict saturated hydraulic conductivity, *Trans. ASAE*, *41*, 983–988.

Romano, N., P. Nasta, G. Severino, and J. W. Hopmans (2011), Using bimodal log-normal functions to describe soil hydraulic properties, *Soil Sci. Soc. Am. J.*, *75*, 468–480.

Schelle, H., S. C. Iden, A. Peters, and W. Durner (2010), Analysis of the agreement of soil hydraulic properties obtained from multistep-outflow and evaporation methods, *Vadose Zone J.*, *9*,1080–1091.

Timlin, D. J., L. R. Ahuja, Y. Pachepsky, R. D. Williams, D. Gimenez, and W. Rawls (1999), Use of Brooks-Corey parameters to improve estimates of saturated conductivity from effective porosity, *Soil Sci. Soc. Am. J.*, *63*, 1086–1092.

Tuller, M., and D. Or (2002), Unsaturated hydraulic conductivity of structured porous media: A review of liquid configuration-based models, *Vadose Zone J.*, *1*, 14–37.

van Genuchten, M. Th. (1980), A closed form equation for predicting the hydraulic conductivity of unsaturated soils, *Soil Sci. Soc. Am. J.*, *144*, 892–898.

Vervoort, R. W., and S. R. Cattle (2003), Linking hydraulic conductivity and tortuosity parameters to pore space geometry and pore-size distribution, *J. Hydrol.*, *272*, 36–49.

Whalley, W. R., G. P. Matthews, and S. Ferraris (2012), The effect of compaction and shear deformation of saturated soil on hydraulic conductivity, *Soil Tillage Res.*, *125*, 23–29.

Wösten, J. H. M., A. Lilly, A. Nemes, and C. Le Bas (1999), Development and use of a database of hydraulic properties of European soils, *Geoderma*, *90*, 169–185.